Available online at www.sciencedirect.com

SciVerse ScienceDirect

Ceramics International 39 (2013) 101–110

CERAMICS INTERNATIONAL

www.elsevier.com/locate/ceramint

Microstructures and tribological properties of vacuum plasma sprayed B_4C–Ni composite coatings

Huiying Zhu, Yaran Niu, Chucheng Lin, Liping Huang, Heng Ji, Xuebin Zheng*

Key Laboratory of Inorganic Coating Materials, Shanghai Institute of Ceramics, Chinese Academy of Sciences, 1295 Dingxi Road, Shanghai 200050, PR China

Received 26 April 2012; accepted 27 May 2012
Available online 13 June 2012

Abstract

A promising wear resistant coating has been fabricated via vacuum plasma spray (VPS) technique by using electroless plating composite powders comprised of B_4C and different amounts of Ni (10 and 20 vol.%). Tribological evaluation from the ball-on-disk test showed that the wear resistance of the composite coatings was superior to that of the pure B_4C coating, and the composite deposit containing 10 vol.% Ni demonstrated the optimum tribological properties. This mainly attributed to the more uniform microstructures of the composite coatings, and the higher thermal conductivity of the composite coating also contributed to its distinguished wear behaviors. For the coatings investigated, the dominant wear mechanism was determined to be oxidation and the formation of a transfer layer on the worn surface.
© 2012 Elsevier Ltd and Techna Group S.r.l. All rights reserved.

Keywords: B_4C–Ni composite coating; Sliding wear; Vacuum plasma spraying

1. Introduction

In many types of industrial machinery, surface damage generated by sliding or abrasive wear limits the life of the components and therefore reduces their durability and reliability [1]. This drives the development of wear-resistant coatings and films that enable to improve the performance of engineering components under different conditions.

Non-oxide ceramic materials, such as boron carbide (B_4C), titanium carbide (TiC), and silicon carbide (SiC), have played an important role in resisting wear and corrosion at either ambient or high temperature [2]. B_4C is a covalently bonded compound and is well-known for its exceptional hardness, which is second only to diamond and c-BN [3,4]. This specific property comes along with other attractive properties such as high melting point, low density and excellent resistance to chemical agents as well as a high neutron absorption cross section [4]. Due to these extraordinary properties, B_4C has been used for lightweight ceramic armors, wear-resistant components such as blasting nozzles and grinding wheels, and coating materials to offer protection for the Tokamak first wall in the nuclear fusion reactors [5,6]. In the case of applying B_4C coating as a wear-resistant material, it seems reasonable to use thick coatings so as to provide effective protection for the base substrate materials [7,8]. In order to make such a thick coating, plasma spraying is considered to be relatively suitable since it has higher deposition rate compared with other methods, such as chemical vapor deposition [9–12], physical vapor deposition [13], sputtering [14–16], pulsed laser deposition [17] and ion beam evaporation techniques [18].

However, dense coatings of B_4C with high bonding strength are not easy to be prepared by plasma spraying, since the intrinsic low thermal conductivity and ductility of B_4C will result in cracks in the coating during spraying [19]. A method to solve this problem is to apply the technology developed in the preparation of B_4C bulk components, where microstructures and mechanical properties of B_4C matrix ceramic materials have been improved by the introduction of second phases [20]. Considering that

*Corresponding author. Tel./fax: +86 21 52414104.
E-mail address: xbzheng@mail.sic.ac.cn (X. Zheng).

0272-8842/$36.00 © 2012 Elsevier Ltd and Techna Group S.r.l. All rights reserved.
http://dx.doi.org/10.1016/j.ceramint.2012.05.101

composite and cermet materials have already been used for numbers of years as a solution to a variety of engineering problems, and the quality of contact between the piled-up splats in plasma-sprayed coatings is influenced by the thermophysical properties of sprayed materials [21], metals such as nickel, copper and aluminum, which are well known for their high thermal conductivity and ductility, have attracted massive interest. If metals are incorporated with B_4C in deposition, heat transfer during spraying will be improved. Moreover, the high thermal conductivity and excellent ductility of metal might also be beneficial to the tribological properties of the coating.

System consisting of carbide particles with metallic binder of Ni has been paid much attention due to its excellent combination of wear resistance and high temperature mechanical properties [22]. Cardoso et al. [23], for instance, have found that the friction coefficient of plasma-sprayed TiC–Ni (15 wt %) coating was much lower than that of the WC–Co coating. As reported by Li et al. [24], the mechanical property and wear-resistant performance of plasma sprayed Cr_3C_2-based coating using Ni-clad Cr_3C_2 powder was outstandingly improved comparing with the coating using mechanically blended Cr_3C_2–NiCr powder. Based on these delightful results, a remarkable improvement in tribological property was expected for plasma sprayed B_4C coating by bringing in Ni as a second phase.

Table 1
Chemical compositions of the electroless nickel plating solutions and corresponding operating conditions.

Powder code	BN10 (90 vol.% B_4C-10 vol.% Ni)	BN20 (80 vol.% B_4C-20 vol.% Ni)
$NiSO_4 \cdot 6H_2O$ (g)	90	200
$N_2H_4 \cdot H_2O$ (ml)	540	1200
$C_4H_4C_6Na_2 \cdot 2H_2O$ (g)	90	200
$C_{10}H_{14}N_2Na_2O_8 \cdot 2H_2O$ (g)	45	100
PbAC (mg)	2.7	6
pH value [a]	13–13.5	13–13.5
Temperature (°C)	92–95	92–95
Volume of solution (l)	5	5
Weighty of primary powder (g)	50	50
Plating time ($_{min}$)	60	60

[a]Adjusting the pH value of the solutions by NaOH.

In this study, electroless plating was chosen to produce B_4C–Ni composite powers, which were subsequently deposited on stainless steel by vacuum plasma spraying. The goal of this work is to examine the wear behaviors of the composite coating comparing with the pure B_4C coating. The relationship between tribological properties and their microstructures were also discussed.

2. Materials and experimental procedure

2.1. Processing of thermal spray feedstock powders

A commercial B_4C powder (W28, Mudanjiang Jingangzuan Boron Carbide Co., Ltd, China) was employed in this work, and the composite powder containing different contents (10 and 20 vol. %) of nickel was prepared by changing the chemical compositions of the electroless nickel plating solutions. The detailed operating conditions are listed in Table 1.

As an example of the B_4C–Ni composite powders, the surface and cross-sectional morphologies of the BN20 powder are shown in Fig. 1. As can be seen, fine nickel particles were homogeneously plated around the surface of the B_4C particles as a dense clad layer, and the cladding thickness was quite uniform. XRD patterns of the composite powders (Fig. 2) reveal that the plated layer was consisted of pure Ni.

2.2. Vacuum plasma spraying process of the coatings

A vacuum plasma spraying (F4-VB, Sulzer-Metco, Switzerland) system was used to deposit coatings from the initial powders following the optimized spraying parameters listed in Table 2. Before deposition, the stainless steel substrate was cleaned and grit-blasted, and NiCrAlY powder (PR2611, Precursor Plasma Powders, China) was deposited as a bond layer prior to spraying the B_4C-based composite coatings.

2.3. Coating characterization

Phase composition and cross-sectional morphologies of both feedstock powders and as-sprayed coatings were

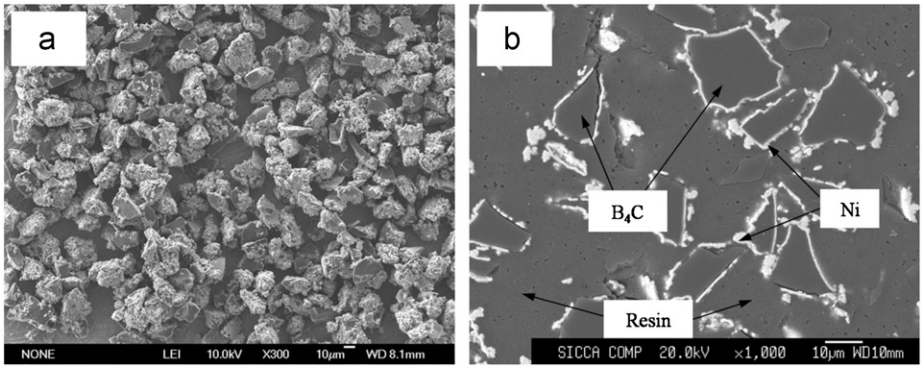

Fig. 1. (a) Surface and (b) cross-sectional morphologies of the BN20 powder

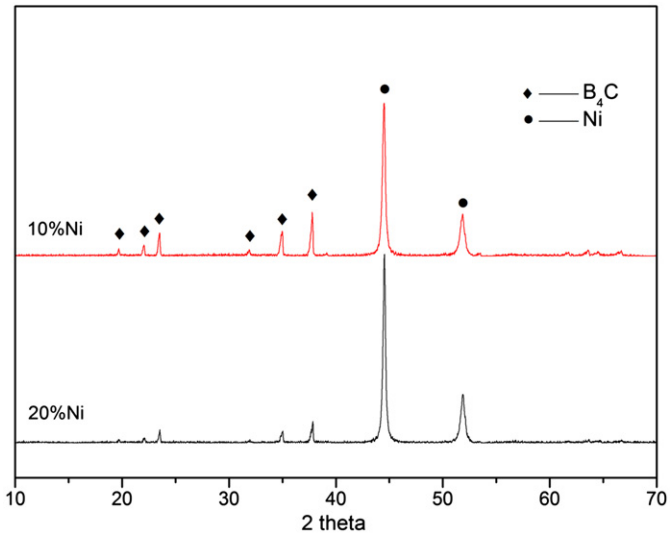

Fig. 2. XRD patterns of the B_4C/Ni composite power.

Table 2
Plasma spraying parameters used for coating deposition.

Parameters	
Current (A)	620
Ar gas flow (slpm)	37
H_2 gas flow (slpm)	13
Carrier gas flow (slpm)	2.5
Powder feed rate (slpm)	22
Spray distance (mm)	220
Pressure (mbar)	400

identified by X-ray diffraction (XRD, CuKα, λ=1.5406 nm, D/Max-2550V, Rigaku, Japan) and scanning electron microscope (SEM, JSM-6700F, JEOL, Japan) equipped with an energy dispersive spectrometer (EDS, INCA ENERGY, UK), respectively. Transmission electron microscope (TEM, JEM-2100F, JEOL, Japan) was employed to investigate the microstructures of the coatings in detail.

Microhardness tests were performed using a microhardness tester (HX-1000, Shanghai Taiming Optical Instrument Company, China), at the load of 500 gf with a dwell time of 15 s. Twenty indentations were made on each sample to obtain an average value of hardness, which were placed in the middle of the cross-sectioned and polished coating samples parallel to the coating/substrate interface. The distance between indentations was kept five times greater than the indentation diagonals to prevent the effects of the stress field of indentations nearby.

Thermal diffusivity (α) was detected by a thermal conductivity meter (LFA 427, NETZSCH, Germany) and specific heat (c_p) was measured by a differential scanning calorimeter (DSC-2C, Perkin Elmer, USA). Based on these two thermophysical parameters, thermal conductivity (λ) of the coating was calculated according to Eq. (1):

$$\lambda = \alpha c_p \rho \quad (1)$$

where ρ is the density of the coating, which was obtained following Archimedes' principle.

2.4. Wear testing

Disk specimens of 60 mm in diameter (as showing in Fig. 3) were deposited with B_4C–Ni composite coatings of 300–500 μm thickness, and the friction and wear properties of these samples were investigated on a Universal Micro-Tribometer tester (UMT-3, CETR, USA), where WC–Co (YG6, Jiaxing JNE Sintered Carbide Company, China) with the hardness of HRA90-92 was used as the ball. Prior to the wear testing, the coating surfaces were polished and the final surface roughness was 0.2 μm. The tests were conducted at room temperature at a sliding speed of 0.5 m/s, with an applied load of 20 N and a sliding distance of 900 m.

The friction coefficients were continuously recorded with sliding distance and directly displayed on the tester. The cross-sectional areas of the worn tracks were obtained by a surface profile-meter (T8000, Hommelwerke, Germany). Based on the diameter and the cross-sectional area of the worn track, volume loss (V) during sliding test was evaluated. Volume wear rate W was determined according to Eq. (2):

$$W = \frac{V}{PL} \quad (2)$$

where P was the normal load applied and L was the sliding distance.

The samples were washed quickly after the wearing test in an ultrasonic bath to remove the entrapped debris before the measurements of volume loss. From six measurements along the track, the average value of the cross-

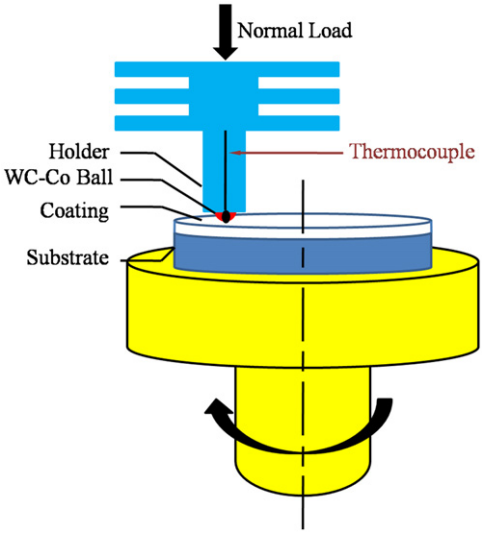

Fig. 3. Schematic of the ball-on-disk tester.

sectional area of each worn track was obtained. During the wear testing, a thermocouple (JNDA 82II, Jingda Instrument, China), as indicated in Fig. 3, was employed to measure the friction temperature, which can be used to perform a sound comparison of the tribological heat generated and concentrated on the contact area for different friction pairs. Morphologies of the worn surfaces and wear debris were characterized using SEM. To insure the reproducibility of the measurements, three repeated tests were conducted under the same conditions for each friction pair.

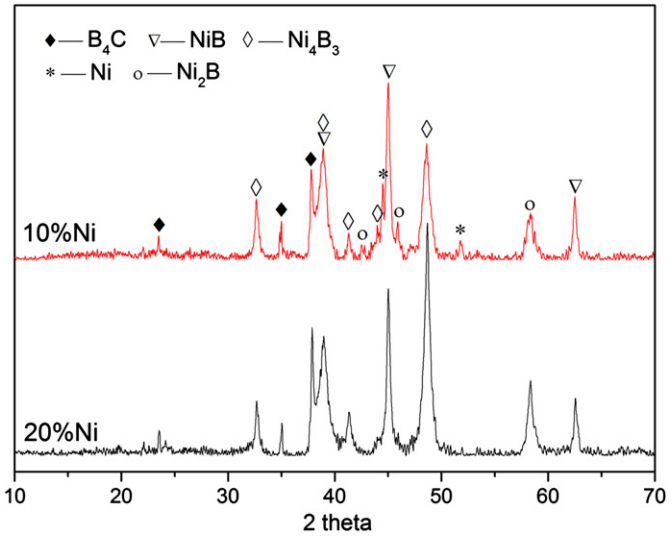

Fig. 4. XRD patterns of the composite coatings.

3. Results and discussion

3.1. Microstructure of coatings

Fig. 4 shows the phase compositions of the B_4C–Ni composite coatings. As can be seen, nickel borides (NiB, Ni_4B_3 and Ni_2B) were obtained during spraying, and due to the limited scattering factor of B_4C, its diffraction peaks were not apparent. Dense microstructures were observed on the cross-sections of the B_4C–Ni composite coatings, as shown in Fig. 5, and the BN10 coating revealed more homogenously dispersed pores with a smaller size comparing with both of the B_4C coating and the BN20 coating.

TEM was employed to gain further information about the microstructures of the B_4C–Ni composite coatings. TEM bright-field images and selected-area electron diffraction (SAED) patterns from the BN20 coating are shown in Fig. 6. The SAED pattern from the Area A in Fig. 6a illustrates single-crystal NiB from the $[1\bar{1}2]$ zone (Fig. 6b), while that from the Area B in Fig. 6a demonstrates nanostructured B_4C grains uniformly dispersing among the boride matrix (Fig. 6c).

EDS (Fig. 7) in conjunction with SEM (Fig. 5) and TEM (Fig. 6) analysis indicate that, with B_4C nano-grains homogeneously distributed among it, nickel borides (NiB, Ni_4B_3 and Ni_2B) obtained during spraying had formed a

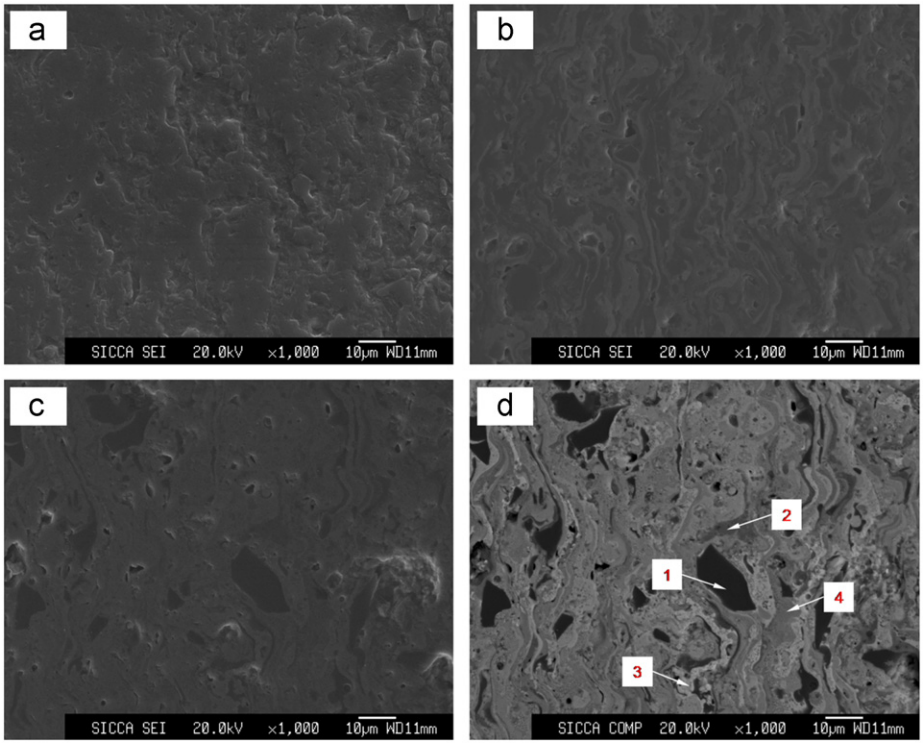

Fig. 5. Cross-sectional morphologies of (a) B_4C, (b) BN10 and (c) (d) BN20 coatings.

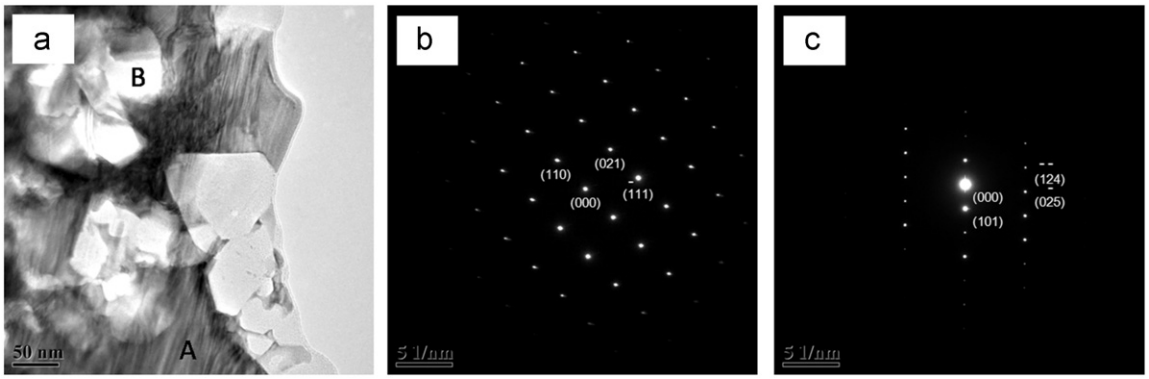

Fig. 6. (a) Typical TEM microstructure of the BN20 coating and SAED pattern taken from (b) Area A and (c) Area B in (a).

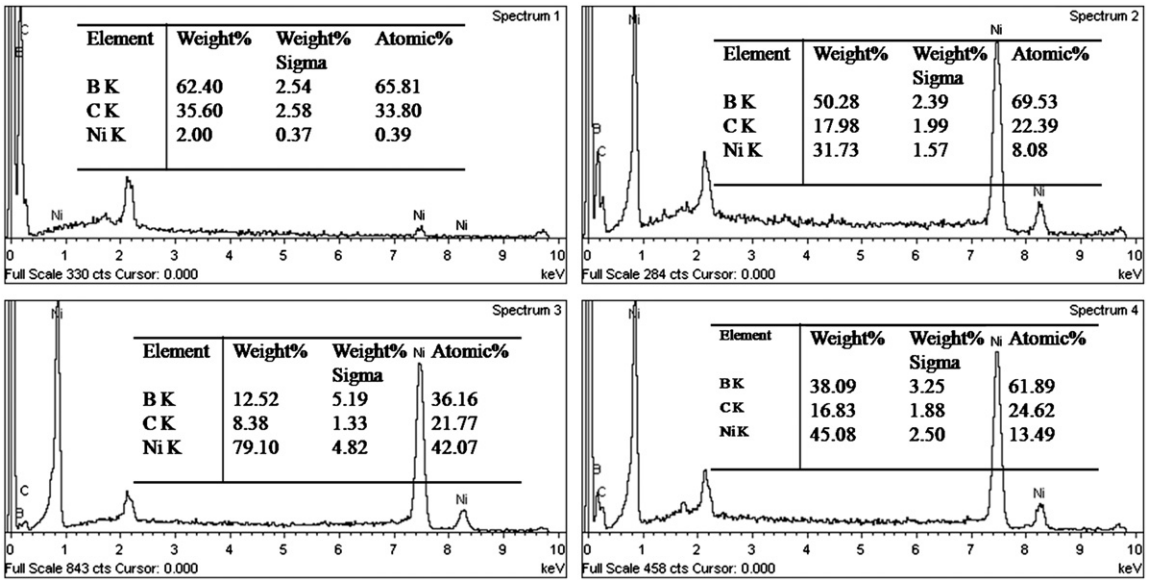

Fig. 7. EDS analysis from the cross-section of the BN20 coating in Fig. 5d.

continuous structure of the electroless plating composite coating.

3.2. Sliding wear behavior

The sliding wear characteristics of as-sprayed coatings against WC–Co alloy were evaluated with an applied load of 20 N and a speed of 0.5 m/s. The variation of friction coefficients for different friction pairs is shown Fig. 8. As can be seen, friction coefficients of the composite coatings behaved in a similar manner (curve a and b in Fig. 8), that is, during the running-in period, the friction coefficient rose rapidly from a low value, and when the steady-stage was reached, it remained almost unchanged. This is in agreement with the variation of friction temperature characterized by the thermocouple equipped to the wear tester (Fig. 3), as shown in Fig. 9. In addition, it is clear that the steady-stage friction coefficient of the composite coating was raised with increasing Ni content, but was still much lower than that of the B_4C coating under the conditions used in the present work (Fig. 10).

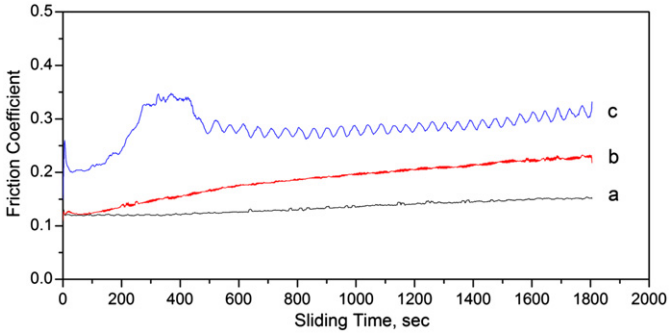

Fig. 8. Friction coefficients of (a) BN10/WC–Co alloy, (b) BN20/WC–Co alloy and (c) B_4C/WC–Co alloy friction pairs depending on time.

Wear rates of the B_4C coating and B_4C–Ni composite coatings after the sliding wear test are shown in Fig. 11. It is observed that wear rates of the composite coatings were remarkably lower than that of the B_4C coating, and the BN10 coating with the minimum wear rate of $0.42 \pm 0.06 \times 10^{-6}\,mm^3\,N^{-1}\,m^{-1}$ exhibited the best wear-resistant properties.

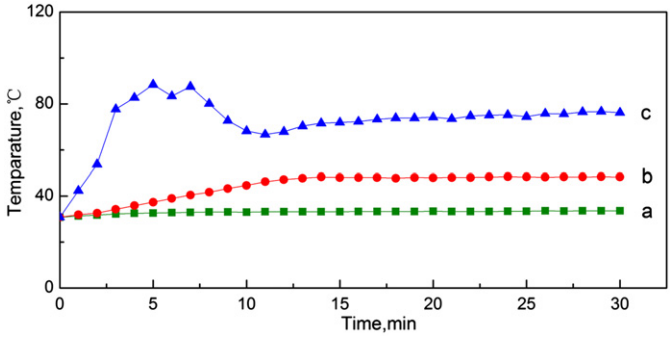

Fig. 9. Measured friction temperatures characterizing frictional heat concentrated in the real contact areas of (a) BN10/WC–Co alloy, (b) BN20/WC–Co alloy and (c) B_4C/WC–Co alloy friction pairs.

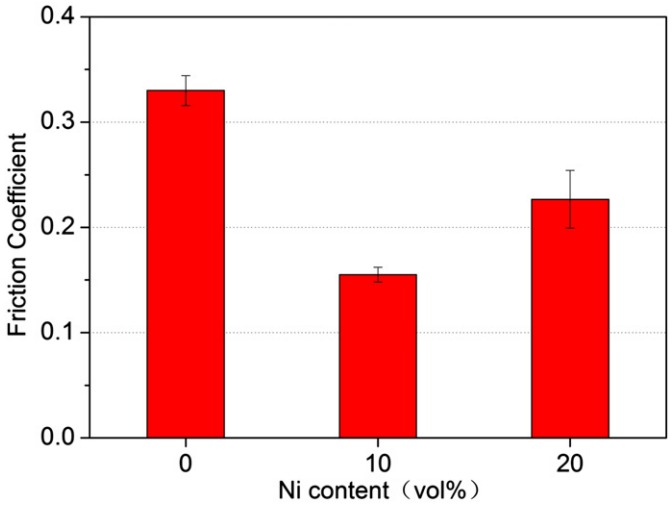

Fig. 10. Friction coefficients of (a) BN10/WC–Co alloy, (b) BN20/WC–Co alloy and (c) B_4C/WC–Co alloy friction pairs.

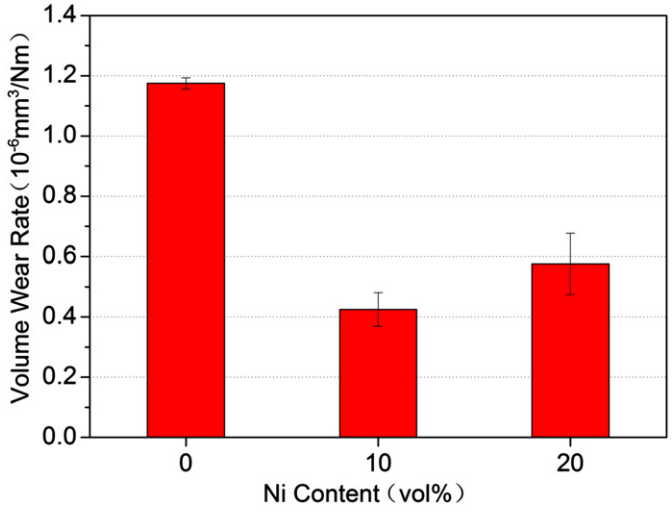

Fig. 11. Volume wear rates of coatings with different amounts of Ni.

3.3. Worn surface and coating failure analysis

In order to investigate the wear mechanisms, worn surface of the coatings was characterized by SEM. As illustrated in Fig. 12a, a discontinuous transfer layer was formed on the worn surface of the composite coating after sliding against WC–Co alloy for 1800 s, just like the B_4C coating (Fig. 12d) [19]. The higher magnification SEM micrographs show that the transfer layer on the worn surface of the BN10 coating remained almost intact after wearing and revealed only a small amount of slight grooves parallel to the sliding direction (Fig. 12b), indicating the occurrence of plastic deformation [25]. Smooth surface was also obtained for the BN20 coating after the wear test (Fig. 12c), however, the transfer layer was not as compact as that in the BN10 coating, and some cracks were observed on it. For both of the composite coatings, no large scale fractures or damages were detected comparing with the B_4C coating (Fig. 12d), and original splat outlines on the worn surface could still be discerned.

EDS analysis revealed that the transfer layer smeared on the worn surface of the BN10 coating, as shown in Fig. 13, was mainly from the WC–Co alloy counterbody materials. The corresponding wear debris was a mixture of flakes and fine particles (Fig. 14a) with a composition similar to that of the transfer layer, as identified by EDS. Transfer layer on the worn surface of the BN20 coating was also predominantly composed of WC–Co alloy and its oxide, but thicker flakes and coarse particles were found in the wear debris for this coating, as presented in Fig. 14b, indicating a severer wear the BN20 coating had experienced comparing with the BN10 coating.

Worn surface of the counterbody balls was also investigated. As shown in Fig. 15, pits (Area A) were observed on the worn surface of WC–Co ball after sliding against BN10 coating for 1800 s. Corresponding EDS analysis from this area demonstrated the presence of oxygen, while the smooth areas surrounding it (Area B) showed the presence of only W, Co and C. In the last few years, a lot of work has been carried out to realize the tribological characteristics of ceramic/metal unlubricated sliding [25–28]. It was suggested that during the ceramic/metal unlubricated sliding wear process, oxidation reactions took place firstly in the real contact areas of the metal surface due to the combined effects of contact stress and frictional heat. Fine debris particles were then generated from fragmentation and detachment of the oxidation regions under repeated cyclic stress, and partially got adherent on the ceramic coating surface to form compacted and protective layers. The transfer layer firmly attached to the coating surface acted as a separation and prevented direct contact between the ceramic/metal counterface during sliding, which hence decreased the wear loss of the ceramic coatings. This proposition was well confirmed in the present work.

3.4. Discussion

3.4.1. Effect of coating microstructures on the sliding wear behaviors

The foregoing results suggest that the wear resistance of the plasma-sprayed B_4C/Ni composite coating was

superior to that of the B_4C coating and the BN10 coating demonstrated the optimum tribological properties, as shown in Fig. 10 and Fig. 11.

As we know, a plasma-sprayed ceramic coating is built up when particles melt, flatten, adhere and solidify on impact with the target substrate [21,26,29,30]. Due to the high cooling rate and thermal mismatch between the ceramic deposit and metal substrate, structural defects like splat interfaces, porosity and microcracks easily appear within the coating, which may degrade the mechanical properties and in turn the wear resistance of coating [31,32]. As shown in Fig. 5, obvious difference in microstructural characteristics between the B_4C–Ni composite coating and B_4C coating was observed: the composite coatings were much denser comparing with the B_4C coating, and the BN10 coating demonstrated the most homogeneous microstructures. Studies have suggested that [33,34], during the wear test, damages usually occur along the pre-existed defects such as pores, microcracks or splat interfaces preferentially under the elevated cyclic and thermal stress, and result in splat spallation or detachment of transfer layer. As a result, pits and microfracture were found on the worn surface of the B_4C coating, while the worn surface of the composite coatings maintained well (Fig. 12).

As reported by Economou et al. [35], the wettability of carbide by the matrix and the carbide–matrix interface strength are also important factors that influence the wear performance of coatings. For the B_4C–Ni composite coatings investigated in this study, chemical reaction had taken place between the dense clad layers of Ni and the well encapsulated B_4C particles during spraying, and a case of NiB_{1-x} that surrounding the B_4C core of each particle was formed, which effectively improved the wettability of the carbide phase by the matrix and led to an enhancement of the carbide–matrix interface strength. The continuous borides skeleton (NiB, Ni_4B_3 and Ni_2B) probably supported the contact load during the sliding wear, while the nano-sized B_4C particles dispersing among it resisted the abrasion from the hard WC–Co alloy, which therefore resulted in the excellent wear performance of the composite coatings.

4. Effect of coating thermo-mechanical properties on the sliding wear behaviors

It is commonly indicated that the wear resistance of a material is closely related to its microhardness, and a high hardness is desirable for both brittle and ductile materials [36]. In this study, however, though the microhardness of the B_4C coating is higher than that of the composite coating (Fig. 16), while sliding against WC–Co alloy, the former coating exhibited lower anti-wear properties. According to Gecim [37] and Yin et al. [27], in an unlubricated sliding process, frictional heat occurs at the real contact areas simultaneously with the wear of materials. Considering the significance of frictional heat transfer during sliding wear process [37] and the high dependence of material hardness on the testing temperature [38,39], we

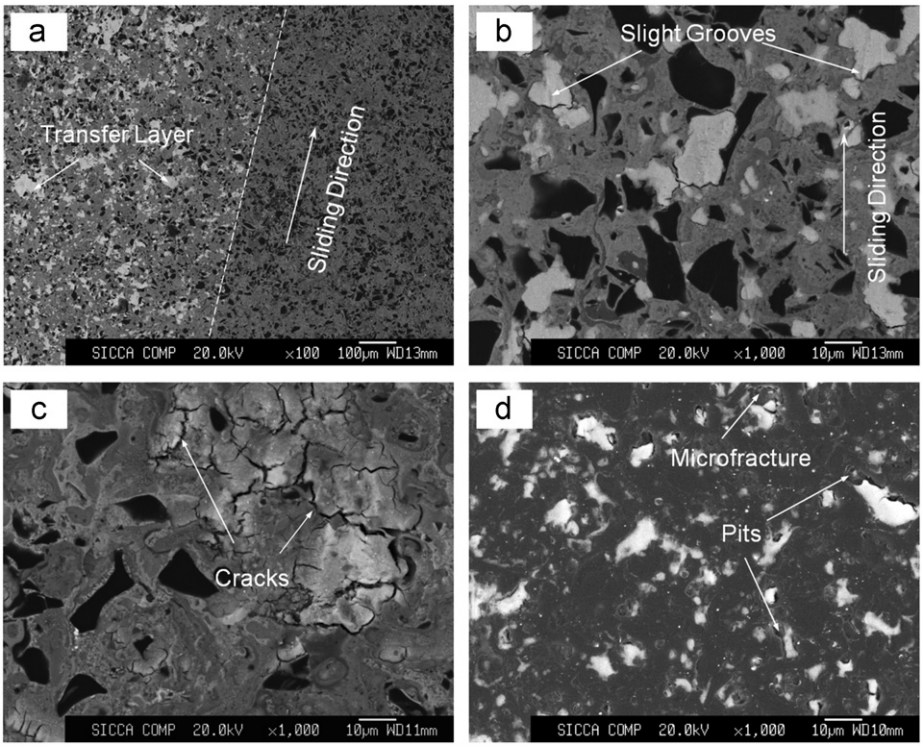

Fig. 12. SEM morphologies of the worn surface of (a) (b) BN10, (c) BN20 and (d) B_4C coatings.

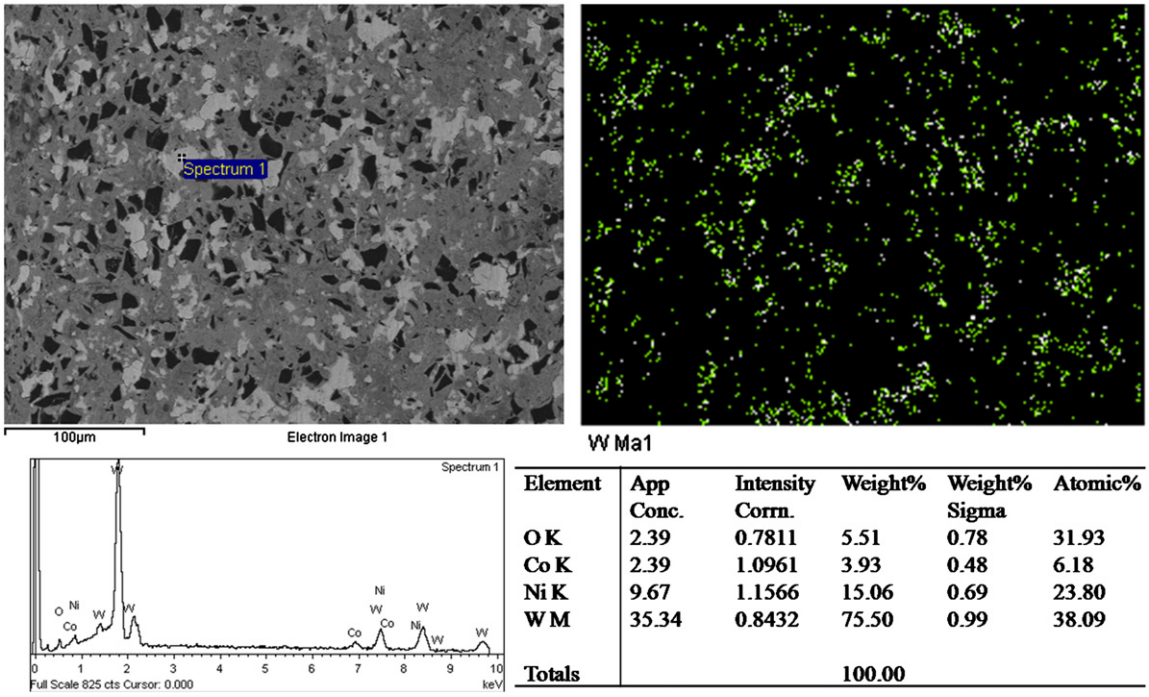

Element	App Conc.	Intensity Corrn.	Weight%	Weight% Sigma	Atomic%
O K	2.39	0.7811	5.51	0.78	31.93
Co K	2.39	1.0961	3.93	0.48	6.18
Ni K	9.67	1.1566	15.06	0.69	23.80
W M	35.34	0.8432	75.50	0.99	38.09
Totals			100.00		

Fig. 13. EDS analysis of the worn surface for the BN10 coating.

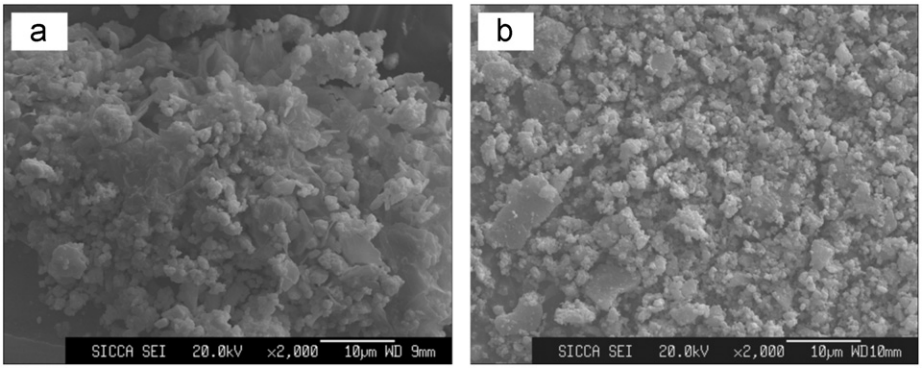

Fig. 14. SEM morphologies of wear debris for (a) BN10/WC–Co alloy and (b) BN20/WC–Co alloy friction pairs.

attribute the higher wear resistance of the composite coating to its better thermal conductivity.

The friction temperature at the measured point on the disk (Fig. 3) was related to the frictional heat generated during the wear test [26]. Due to the higher thermal conductivity of the BN10 coating (Fig. 17), the accumulation of frictional heat at the real contact areas was alleviated, which therefore resulted in low and constant friction temperature of the coating through the entire testing period, as shown in Fig. 9. According to Tao et al. [26], this well-established thermal equilibrium was considered to be helpful to maintain the transfer layer on the worn surface during the friction process to provide effective protection for the underlying coating (Fig. 12), which in turn contributed to the better wear resistance for the BN10 coating, comparing with both of the B_4C coating and the BN20 coating.

On the other hand, it has been demonstrated that local softening, which aids local welding and plastic flow of material, might happen due to the concentration of frictional heat [37]. Besides, as the temperature of the contact surface is increased, so is the contribution of thermal stress [40], and the effective yield stress of materials will be substantially decreased [37]. Dzhemelinskii and Thvenot et al. [38,39] pointed out that hardness of B_4C showed strong dependence on its surface temperature and decreased with increasing temperature. It is then concluded that although the microhardness of the B_4C–Ni composite coating was lower than that of the B_4C coating, its higher thermal conductivity effectively facilitated the dissipation of frictional heat and alleviated the reduction of hardness due to the accumulated frictional heat.

Despite the differences in friction coefficients and wear rates, the main wear mechanisms for both the B_4C coating

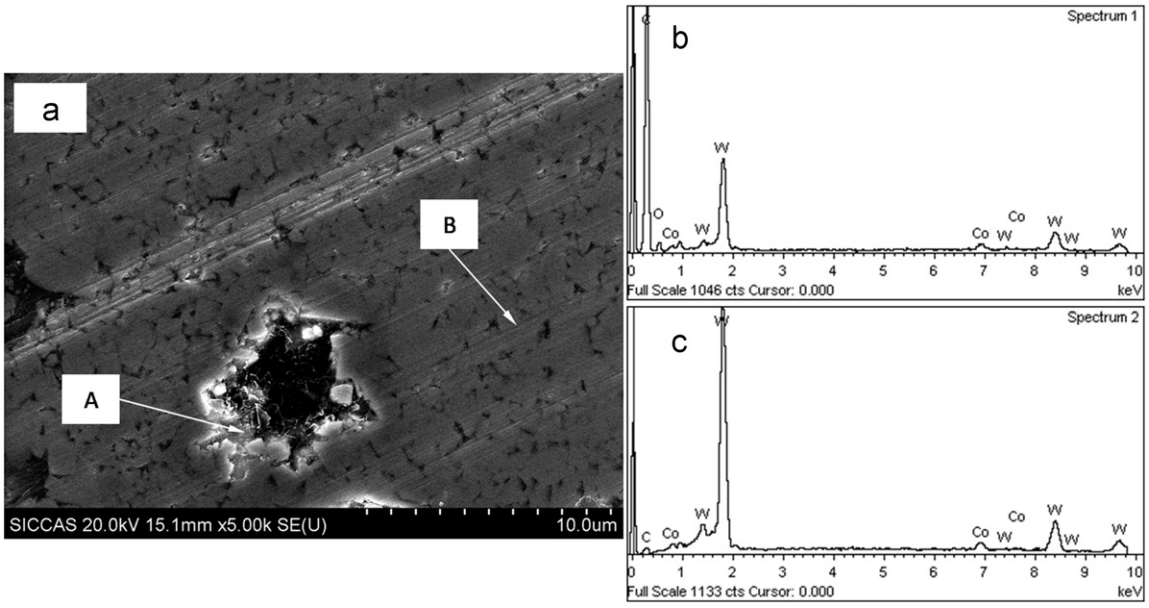

Fig. 15. (a) SEM morphology of the worn surface for the WC–Co ball sliding against BN10 coating and corresponding EDS analysis from (b) Area A and (c) Area B in (a).

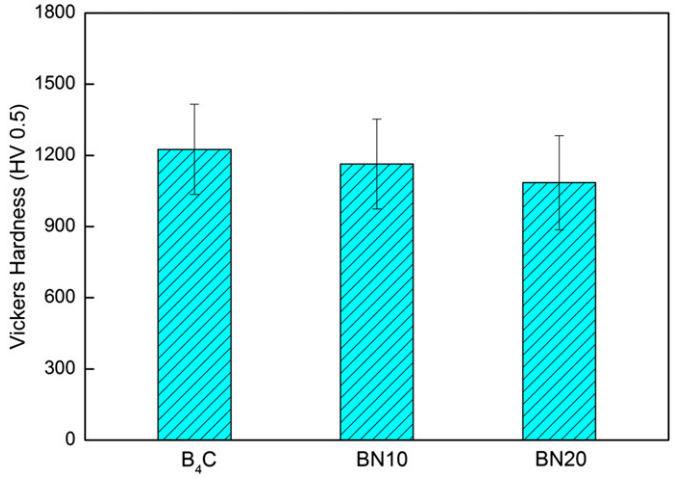

Fig. 16. Microhardness of coatings with different amounts of Ni.

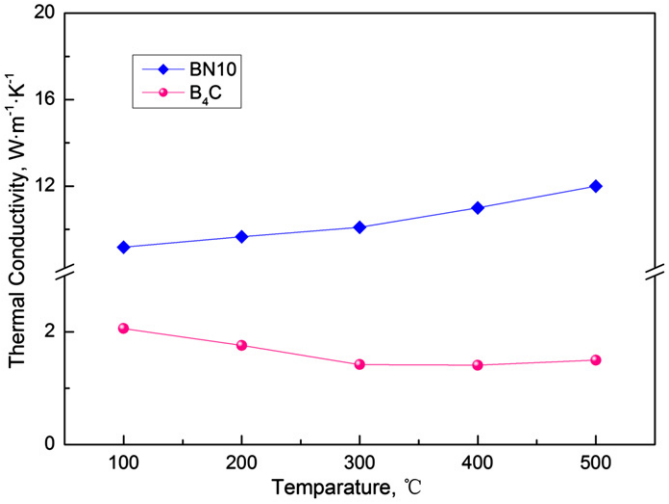

Fig. 17. Thermal conductivity of as-sprayed coatings.

and the composite coatings sliding against WC–Co alloy were oxidation and tribofilm wear [19], as was evident from the presence of W, Co and O on the worn surface of the coatings (Fig. 13).

5. Conclusion

B_4C–Ni composite powder was produced by electroless plating process, and then deposited on stainless steel via vacuum plasma spraying. Friction and wear properties of the composite coating sliding against WC–Co alloy were evaluated using a ball-on-disk configuration at room temperature.

The results obtained showed that nickel borides were produced during spraying in the composite coating, which improved the wettability of the carbide phase by the matrix and led to an enhancement of the carbide–matrix interface strength. Due to the more homogenous microstructure and effective protection from the compact transfer layer on the worn surface, the B_4C–Ni composite coating exhibited both lower friction coefficient and volume wear rate than those of the pure B_4C coating while matching with WC–Co alloy under the conditions used in the present study. The improvement in wear resistance of the B_4C/Ni composite coating was also attributed to its higher thermal conductivity, since the concentration of frictional heat was alleviated in the real contact areas. For the coatings investigated, the dominant wear mechanisms were a mixture of oxidation and tribofilm wear.

Acknowledgments

This work was jointly supported by the National Natural Science Foundation (for Young Scholar) of China under grant 51102267, Shanghai Science and Technology R&D Fund under grant 11ZR1442100.

References

[1] L. Prchlik, S. Sampath, J. Gutleber, G. Bancke, A.W. Ruff, Friction and wear properties of WC–Co and Mo–Mo_2C based functionally graded materials, Wear 249 (2001) 1103–1115.
[2] H. Li, K.A. Khor, L.G. Yu, P. Cheang, Microstructure modifications and phase transformation in plasma-sprayed WC-Co coatings following post-spray spark plasma sintering, Surface and Coatings Technology 194 (2005) 96–102.
[3] H.R. Salimijazi, T.W. Coyle, J. Mostaghimi, L. Leblanc, Microstructure of vacuum plasma-sprayed boron carbide, Journal of Thermal Spray Technology 14 (2005) 268–362.
[4] B.-S. Lee, S. Kang, Low-temperature processing of B_4C-Al composites via infiltration technique, Materials Chemistry and Physics 67 (2001) 249–255.
[5] H. Lee, R.F. Speyer, Pressureless sintering of boron carbide, Journal of the American Ceramic Society 86 (2003) 1468–1473.
[6] H. Greuner, M. Balden, B. Boeswirth, Evaluation of vacuum plasma-sprayed boron carbide protection for the stainless steel first wall of WENDELSTEIN 7-X, Journal of Nuclear Materials 329–333 (2004) 849–854.
[7] J. Kitamura, S. Usuba, Y. Kakudate, H. Yokoi, K. Yamamoto, A. Tanaka, Structure and mechanical properties of boron carbide coatings formed by electromagnetically accelerated plasma spraying, Diamond and Related Materials 12 (2003) 1891–1896.
[8] K. Holmberg, H. Ronkainen, A. Matthews, Tribology of thin coatings, Ceramics International 26 (2000) 787–795.
[9] J.C. Oliveira, M.N. Oliveira, O. Conde, Structural characterization of B_4C films deposited by laser-assisted CVD, Surface and Coatings Technology 80 (1996) 100–104.
[10] K.W. Lee, S.J. Harris, Boron carbide films grown from microwave plasma chemical vapor depositon, Diamond and Related Materials 7 (1998) 1539–1543.
[11] J.C. Oliveira, P. Paiva, M.N. Oliveira, O. Conde, Laser-assisted CVD of boron carbide at atmospheric pressure, Applied Surface Science 138–139 (1999) 159–164.
[12] S. Lee, J. Mazurowski, G. Ramseyer, P.A. Dowben, Characterization of boron carbide thin films fabricated by plasma enhanced chemical vapor deposition from boranes, Journal of Applied Physics 72 (1992) 4925–4933.
[13] K. Jagannadham, T.R. Watkins, M.J. Lance, L. Riester, R.L. Lemaster, Laser physical vapor deposition of boron carbide films to enhance cutting tool performance, Surface and Coatings Technology 203 (2009) 3151–3156.
[14] A. Lousa, E. Martínez, J. Esteve, E. Pascual, Effect of ion bombardment on the properties of B_4C thin films deposited by RF sputtering, Thin Solid Films 355–356 (1999) 210–213.
[15] M.L. Wu, J.D. Kiely, T. Klemmer, Y.T. Hsia, K. Howard, Process-property relationship of boron carbide thin films by magnetron sputtering, Thin Solid Films 449 (2004) 120–124.
[16] E. Pascual, E. Martínez, J. Esteve, A. Lousa, Boron carbide thin films deposited by tuned-substrate RF magnetron sputtering, Diamond and Related Materials 8 (1999) 402–405.
[17] F. Kokai, M. Taniwaki, K. Takahashi, Laser ablation of boron carbide: thin-film deposition and plume analysis, Diamond and Related Materials 10 (2001) 1412–1416.
[18] H. Suematsu, K. Kitajima, T. Suzuki, W. Jiang, K. Yatsui, Preparation of polycrystalline boron carbide thin films at room temperature by pulsed ion-beam evaporation, Applied Physics Letters 80 (2002) 1153–1155.
[19] H.Y. Zhu, Y.R. Niu, C.C. Lin, L.P. Huang, H. Ji, X.B. Zheng, Fabrication and tribological evaluation of vacuum plasma sprayed B_4C coating, Journal of Thermal Spray Technology. In preparation.
[20] J.L. Sun, C.X. Liu, C.Y. Duan, Effect of Al and TiO_2 on sinterability and mechanical properties of boron carbide, Materials Science and Engineering A: Structural Materials: Properties, Microstructure and Processing 509 (2009) 89–93.
[21] P. Fauchais, M. Fukumoto, A. Vardelle, M. Vardelle, Knowledge concerning splat formation: an invited review, Journal of Thermal Spray Technology 13 (2004) 337–360.
[22] J.E. Cho, S.Y. Hwang, K.Y. Kim, Corrosion behavior of thermal sprayed WC cermet coatings having various metallic binders in strong acidic environment, Surface and Coatings Technology 200 (2006) 2653–2662.
[23] R.J.C. Cardoso, M.A. Ashworth, M.H. Jacobs, Wear behavior of plasma sprayed TiC-15% Ni coatings, Surface Treatment: Computer Methods and Experimental Measurements 17 (1997) 381–389.
[24] J.F. Li, C.X. Ding, Improvement in the properties of plasma-sprayed chromium carbide coatings using nickel-clad powders, Surface and Coatings Technology 130 (2000) 15–19.
[25] X.H. Lin, Y. Zeng, C.X. Ding, P.Y. Zhang, Tribological behavior of nanostructured Al_2O_3-3 wt% TiO_2 coating against steel in dry sliding, Tribology Letters 17 (2004) 19–26.
[26] S.Y. Tao, Z.J. Yin, X.M. Zhou, C.X. Ding, Sliding wear characteristics of plasma-sprayed Al_2O_3 and Cr_2O_3 coatings against copper alloy under severe conditions, Tribology International 43 (2010) 69–75.
[27] Z.J. Yin, S.Y. Tao, X.M. Zhou, C.X. Ding, Tribological properties of plasma sprayed Al/ Al_2O_3 composite coatings, Wear 263 (2007) 1430–1437.
[28] G.W. Stachowiak, G.B. Stachowiak, A.W. Batchelor, Metallic film transfer during metal-ceramic unlubricated sliding, Wear 132 (1989) 361–381.
[29] R. McPherson, The relationship between the mechanism of formation, microstructure and properties of plasma-sprayed coating, Thin Solid Films 83 (1981) 297–310.
[30] R.W. Smith, R. Knight, Thermal spraying I: powder consolidation-from coating to forming, JOM Journal of the Minerals Metals and Materials Society 47 (1995) 32–39.
[31] S. Safai, H. Herman, Microstructural investigation of plasma-sprayed aluminum coating, Thin Solid Films 45 (1977) 295–307.
[32] R. Mcpherson, B.V. Shafer, Interlamellar contact within plasma-sprayed coatings, Thin Solid Films 97 (1982) 201–204.
[33] R. Vijande-Diaz, J. Belzunce, E. Fernandez, A. Rincon, M.C. Pérez, Wear and microstructure in fine ceramic coatings, Wear 148 (1991) 221–233.
[34] P.P. Psyllaki, M. Jeandin, D.I. Pantelis, Microstructure and wear mechanism of thermal-sprayed alumina coatings, Materials Letters 47 (2001) 77–82.
[35] S. Economou, M. De Bonte, J.P. Celis, Tribological behavior of TiC/TaC-reinforced cermet plasma sprayed coatings tested against sapphire, Wear 185 (1995) 93–110.
[36] Y. Wang, S. Jiang, M.D. Wang, S.H. Wang, T.D. Xiao, P.R. Strutt, Abrasive wear characteristics of plasma sprayed nanostructured alumina/titania coatings, Wear 237 (2000) 176–185.
[37] B. Gecim, Transient hot spot temperatures at a sliding ceramic contact including surface coating effects, Wear 123 (1988) 59–76.
[38] V.V. Dzhemelinskii, M.S. Koval'chenko, G.N. Makarenko, Indenter materials for high-temperature hardness measurement, Powder Metallurgy and Metal Ceramics 12 (1973) 168–170.
[39] F. Thvenot, Boron carbide-a comprehensive review, Journal of the European Ceramic Society 6 (1990) 205–225.
[40] J.F. Li, C.X. Ding, J.Q. Huang, P.Y. Zhang, Wear mechanism of plasma-sprayed Cr_3C_2-NiCr against TiO_2 coating, Wear 211 (1977) 177–184.